OPEN ACCESS

Saudi Journal of Civil Engineering

Abbreviated Key Title: Saudi J Civ Eng
ISSN 2523-2657 (Print) |ISSN 2523-2231 (Online)
Scholars Middle East Publishers, Dubai, United Arab Emirates
Journal homepage: https://saudijournals.com/journal/sjce/home

Original Research Article

Flexural Behavior of One-Way Concrete Slabs Reinforced with GFRP Bar under Four-Point Bending Load

Ahmed Abdallah Altayeb[1,2], Salih Alhadi M. Ahmed[1,3], Bashir H. Osman[2*], Eltayeb Abdellatif A. Habib[1]

[1]Civil Engineering Department, College of Engineering, University of Bahri, Khartoum, Sudan
[2]Civil Engineering Department, College of Engineering, University of Sinnar, Sinnar, Sudan
[3]Civil Engineering Department, Sudan University of Science and Technology, Khartoum, Sudan

DOI: https://doi.org/10.36348/sjce.2025.v09i08.001 | **Received:** 04.07.2025 | **Accepted:** 05.09.2025 | **Published:** 08.09.2025

***Corresponding author:** Bashir H. Osman
Civil Engineering Department, College of Engineering, University of Sinnar, Sinnar, Sudan

Abstract

This study aims to investigate the flexural behavior of simply supported one-way reinforced concrete (RC) slabs constructed with high-strength concrete (HSC) and normal-strength concrete (NSC), reinforced with either glass fiber reinforced polymer (GFRP) bars or conventional steel reinforcement. Four large-scale reinforced concrete (RC) slabs were tested under four-point bending. The failure and cracking loads, deflection, crack patterns, and failure modes were considered as main parameters. Results showed that GFRP-reinforced slabs (both NSC and HSC) had higher deflections by 2.60 times and lower ultimate loads by 21.0% to 32.0% compared to steel-reinforced slabs. GFRP-reinforced specimens also experienced sudden failure due to bar rupture and exhibited wider cracks. The experimental results compared with those from analytical predictions based on ACI 440, CAN/CSA S806, and Eurocode 2, the results were in accordance. While CSA S806-12 slightly underestimated cracking loads for HSC-GFRP slabs, it provided accurate mid-span deflection estimates. Eurocode 2 predictions for crack widths were within 10% of the values observed.

Keywords: GFRP; RC Slab; flexural behaviors; HSC; failure modes.

1. INTRODUCTION

Glass fiber reinforced concrete (GFRC), introduced about two decades ago, is a modern material in civil engineering. It has gained widespread use due to its lightweight nature, which helps reduce construction costs and enhances economic efficiency in building projects [1]. FRP materials offer a practical and efficient substitute for steel reinforcement in concrete structures, due to their differing physical and mechanical characteristics from those of steel [2]. Fiberglass composites provide several benefits such as cost-effective production, simple fabrication, reduced weight, and a superior strength-to-weight ratio [3]. Research over the past 15 years has consistently shown that steel fibers are less prone to corrosion than traditional steel bars. [4-7]. GFRP-reinforced concrete members have lower strength and greater deflection compared to steel-reinforced ones, according to experimental studies [8-10]. GFRP rebars have a lower modulus of elasticity, causing them to deflect more under identical loads and span lengths. [11,12]. After cracking, the flexural stiffness of GFRP-reinforced concrete slabs decreases, resulting in greater deflection [13]. GFRP bars embedded in (HSC) demonstrated better performance in terms of deflection compared to those embedded in (NSC) [14]. On the other hand**,** Some researchers found that GFRP slabs have higher ultimate load capacity and better fatigue performance than steel slabs [15-17].

FRP-reinforced concrete members typically show greater deflections and strains than steel-reinforced ones due to FRP's lower modulus of elasticity and different bond behavior [18,19]. GFRP-reinforced elements tend to develop wider cracks than steel-reinforced elements [20,21]. FRP-reinforced concrete members show linear behavior both before and after cracking, but with much lower stiffness after cracking [18]. (HSC) improved both the ultimate-load capacity and initial shear cracking load [22]. Another study found that GFRP-reinforced concrete slabs have fewer cracks, but with larger crack widths [13]. Cracks in GFRP-reinforced concrete slabs form earlier and are wider than in steel-reinforced slabs due to GFRP's lower stiffness, lack of yielding, and weaker bond with concrete. Crack

spacing is wider, and crack width is influenced by bar diameter and surface finish [19,23,24].

Steel-reinforced slabs showed ductile flexural failure with steel yielding before concrete crushing, while GFRP-reinforced slabs exhibited brittle failure governed by concrete crushing, with no reinforcement yielding [25,19,10,15,26,24].

The observed failure modes in the tested GFRP-reinforced slabs included shear-compression failure, diagonal tension failure, and bond or anchorage failure [22]. The flexural behavior of FRP-reinforced members depends on the failure mode, either concrete crushing or FRP rupture, which is determined by comparing the FRP reinforcement ratio to the balanced reinforcement ratio [27].

For conventional concrete, the strains in the FRP rebars rose almost linearly with the applied load after the onset of cracking [28,29]. Ultra-high-performance fiber-reinforced concrete shows nonlinear load–strain behavior, with gradual early strain increase due to its strain-stiffening properties [30]. Other analysis used by [31] concluded that increasing concrete strength from 95 to 117 MPa had little effect on concrete strain under the same applied load. Compared to steel-reinforced concrete, strain in smooth GFRP-reinforced concrete increased by about 44%, and in sand-coated GFRP-reinforced concrete by about 14% [32].

Despite extensive research on the flexural behavior of reinforced concrete (RC) elements over the past two decades, most studies have concentrated on steel reinforcement. There is limited research on simply supported one-way slabs reinforced with glass fiber-reinforced polymer (GFRP), particularly when using high-strength concrete (HSC) and normal-strength concrete (NSC). This paper experimentally investigates the flexural performance of such slabs, considering various GFRP reinforcement ratios (pf/pfb). Key aspects such as load-deflection response, cracking behavior, failure mechanisms, and moment capacity are investigated. The findings are compared with predictions from established design codes such as ACI 440.1R, CSA S806, and other relevant standards codes to evaluate their applicability and accuracy for GFRP-reinforced slabs using both HSC and NSC.

2. Experimental Program

Four simply supported concrete slabs (750 mm × 1500 mm × 125 mm) were tested under four-point bending to evaluate the performance of normal-strength (NSC) and high-strength concrete (HSC) slabs reinforced with steel and GFRP bars. The study measured ultimate load capacity, crack patterns, failure modes, ultimate deflection, and strains in both concrete and reinforcement.

2.1 Materials properties

GFRB bar: Reinforcement of the slabs was achieved using glass fiber-reinforced polymer (GFRP) bars having a nominal diameter of 10 mm, which similar to those used by Yoo, D.-Y., N. Banthia, *et al.,* [12], the properties are summarized in Table 1

Table 1: Properties of GFRP bar

Material	Normal Diameter (mm)	Nominal Area (mm2)	Mas per meter run (gm/m)	Ultimate Load (kN)	Ultimate Tensile Strength (Mpa)	Max. Strain
GFRP	10	78.57	138	80.72	1027.36	0.0258

Steel: High tensile deformed steel bar grade 500 confirming to BS 4449 was used for the experimentation. The mechanical properties are summarized in Table 2.

Silica Fume: For the preparation of high-strength concrete, silica fume was supplied as a dry powder and incorporated into the mixture during batching (Sika Egypt Construction Chemicals).

Table 2: Mechanical properties of Reinforcements

Type	Yield point MPa	Tensile strength MPa	Young modulus GPa	Strain
Grade 500	503.5	634	205	0.0025

A superplasticizer (SikamentR-163M from Sika Egypt) was used to improve the workability of high-strength concrete. Two trial mix compositions similar to those used by [33], detailed in Tables 3 and 4, were prepared using separately weighed constituents and mixed in a 400 kg capacity concrete mixer for 4 minutes as shown in Figure 1. Mechanical vibration was applied for compaction to reduce voids. Slump tests were conducted to confirm target workability. After 24 hours, specimens were demolded, water-cured, and tested at room temperature at designated ages, as shown in Figure 2.

Table 3: Mix proportion for Normal (N) and High (H) performance concrete

Mix (kg/m^3)	Cement	Silica Fume	Sand	Aggregate			Water	Super Plastizer/L
				5MM	10MM	20MM		
NSC	416	0	721	0	338	790	207	0
HSC	400	44	710	393	797	0	140	7.9

Unconfined compressive strength was evaluated by casting six 150 mm cube specimens for each mix, with tests conducted on three samples after 7 days and the remaining three after 28 days of water curing, as presented in Table 4.

Table 4: Cubes designation

No.	Cube designation	No. of cubes	Date of Tested		Additive	Mix Grade
			7 days	28 days		
1	C1(control)	6	3	3	-	30
2	C1.1(control)	6	3	3	Silica Fume	70

Figure 1: Pan mixer

Figure 2: Conduct of concrete cubes test

2.2 Slab details

Four reinforced concrete slabs (S30, S70, F30, F70) were tested under four-point bending to assess flexural behavior. Each slab measured 750 mm × 1500 mm × 125 mm with 25 mm clear cover. Control slabs S30 and S70 were reinforced with 10 steel bars and had concrete grades 30 and 70, respectively as shown in Figure 3& Figure 4. Slabs F30 and F70 used GFRP reinforcement. Slab F30 was over-reinforced (ρf/ρfb > 1.0), while other slabs were designed to be tension-controlled, (ρf/ρfb < 1.0) according to CSA S806-12 [34] as shown in Table 5.

Table 5: Slabs detail

No.	Slab designation	specification				
		Type of bar	Bar size (T)	Additive	Mix Grade	$Pf\ /pfb$
1	S30 (control)	steel	10	-	30	0.33
2	S70 (control)	steel	10	Silica Fume	70	0.19
3	F30	GFRP	10	-	30	1.47
4	F70	GFRP	10	Silica Fume	70	0.82

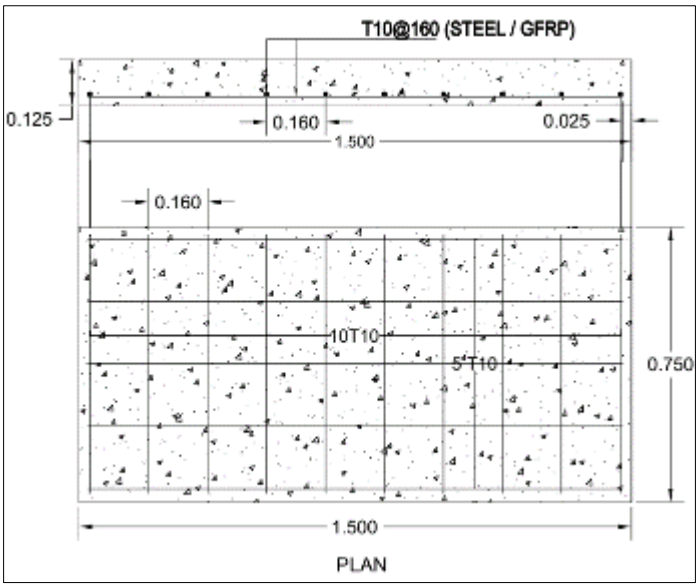

Figure 3: Details of steel / GFRB diagram

Figure 4: Actual Details of steel / GFRP

2.3 Test Setup and specimen preparation

Formwork was constructed using 20 mm thick black plywood panels as shown in Figure 5, assembled to match the slab dimensions. Internal surfaces were oiled to ease demoulding. The steel reinforcement cage was made in the lab using deformed bars, cut with an electric hacksaw, and tied with spring steel ties spaced at 160 mm. Concrete spacers ensured proper cover, and 12 mm bent bars were used as lifting anchors for safe slab handling as shown in Figure 6.

Figure 5: Formwork used for slabs

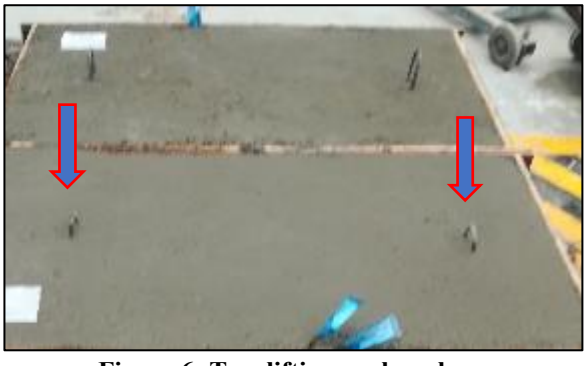

Figure 6: Two lifting anchors bars

2.4 Attachment of strain gauges

Strain measurements were taken using electrical-resistance strain gauges. Two FLAB-6-11 gauges (6 mm × 2.2 mm, 120 Ω, -10°C to +100°C) from Tokyo Measuring Instruments were installed on the longitudinal reinforcement at the slab edges and mid-span as shown in Figure 7. Additionally, PL-60-11 gauges (60 mm × 1.0 mm, 120 Ω, +10°C to +80°C) were

placed on the concrete slab's top surface as illustrated in Figure 8. Gauges were bonded with specialized adhesive, sealed with urethane, tape, and rubber to prevent moisture ingress, and the wiring was protected during casting to ensure accurate and reliable readings.

Figure 7: Attaching the strain gauges to the GFRP and Steel bars

Figure 8: Strain gauges attached on the top concrete surfaces

2.5 Casting of concrete

Concrete was poured directly into the formwork and compacted using internal vibrators, with special attention around the strain gauges. After vibration, the surface was trowelled smooth. Concrete cubes were also cast during the pour, demolded after 24 hours, and placed in a curing tank for strength testing. A slump test conducted on-site yielded a value of 105 mm, confirming acceptable workability. The completed slabs, supported by timber cross members for formwork stability, were cured by continuous water spraying and covered with wet burlap to maintain moisture as shown in Figure 9 and 10.

Figure 9: Specimens preparation

Figure 10: Slabs Curing

2.6 Experimental Configuration and Instrumentation

After the curing process had concluded, the slab was transported by crane to the location of the mechanical testing setup as shown in Figures 11. Experimental testing was conducted on the slabs through a four-point loading configuration, as illustrated in Figures 12 and 13. The load was applied through a 125 × 65 mm steel I-beam subjected to two pieces of a 50mm Round structural steel solid bars, which served to transfer the load from a 50 Ton capacity hydraulic jack directly to the mid-span of the slab

Figure 11: Transported of slab

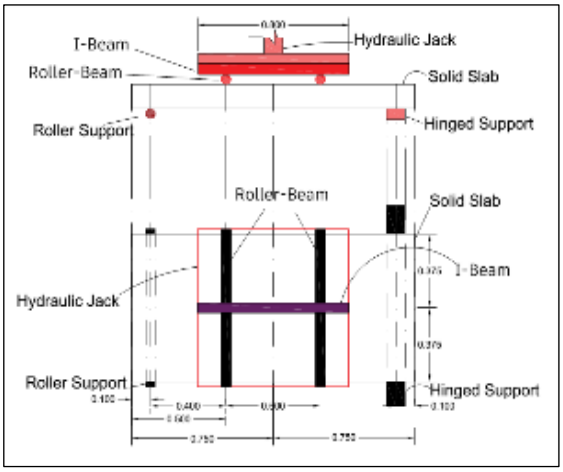

Figure 12: Four-point loading Set-up diagram

Figure 13: Four-point loading Set-up Test

LVDTs were used to measure deflection and crack width during testing (Figure 14). Deflections were recorded at mid-span and edge of slab, while crack widths were measured at the slab's long side. Data on load, deflection, crack width, and strain were collected using a CLT5000 controller. A 500 KN load cell applied incremental loading at 300 kg/s until failure. Initial crack loads were recorded, and crack patterns were marked on the slab surfaces.

Figure 14: LVDTs location to measure deflection and crack width during the test

3. Calculation procedures

3.1. Flexural Capacity

In this study, the Crack moment (*Mcr*) and the Nominal moment capacity (*Mn*) were calculated using formulations in the CSA S806-12 code as the following equations

$Mcr = \frac{fr*Ig}{yt}$ (1)

where: $fr = 0.6\lambda\sqrt{fc'}$

$M_n = \alpha_1 \beta 1c$ fc'.bc($h_{0f} - \beta 1c/2$)bh^2_{bf} *for* $p_f \geq p_{fb}$ (2)

$M_n = Af.\varepsilon f.Ef\ (h_{0f} - \beta c/2)$ *for* $pf < pfb$ (3)

where: $\alpha_1 = 0.85\text{-}0.0015\ fc' \geq 0.67$, $\beta 1 = 0.97 - 0.0025\ fc' \geq 0.67$

$p_f = A_f/bd$,

$p_{fb} = \alpha_1\ \beta 1(fc'/f_{fu})(\varepsilon_{cu}/(\varepsilon_{cu} + \varepsilon_{fu}))$, $p_{f} = Af/bd$, ε_{cu}: = 0.0035

3.2. crack width

Crack width calculations in this study were based on the provisions outlined in CSA S6-06 [41], ACI 440.1R-06 [27] and EURO EN 1992-1-1:2004 code [42] as the following equations. According to CSA S6-06, Equation (4) is used to determine the crack width in FRP-reinforced one-way concrete slabs.

$$w_{cr} = 2\frac{f_f}{E_f}\frac{h_2}{h_1}k_b\sqrt{d_c^2 + (s/2)^2} \quad (4)$$

ACI 440.1R-06 provides Equation 5 for calculating the crack width in GFRP-reinforced concrete elements as follows:

$$w = 2\frac{f_f}{E_f}\beta k_b\sqrt{d_c^2 + \left(\frac{s}{2}\right)^2} \quad (5)$$

$$\beta = \frac{h - kd}{d(1-k)}$$

$$k = \sqrt{2\rho_f n_f + (\rho_f n_f)^2} - \rho_f n_f$$

$$f_f = \frac{M_{DL+LL}}{A_f d(1 - k/3)}$$

$dc = h - d$

Eurocode2 [42] provides guidelines for calculating the crack width in GFRP-reinforced concrete elements. The empirical equation for maximum crack width is:

$wk = S_{r,max}(\varepsilon_{sm} - \varepsilon_{cm})$ (6)

$\varepsilon_{sm} - \varepsilon_{cm} = \sigma s - k_t\frac{f_{ct,eff}}{p_{p,eff}}(1 + \alpha_{e*}p_{p,eff})/E_s \geq 0.6\,\sigma s/Es$

E_s/E_{cm}, f_{ctm} =0.3fck $^{(2/3)}$ ≤ C50/60, f_{ctm} = 2.12 ln (1+ fcm /10) >C50/60, fcm = fck +8 (MPA)

E_{cm} = 22(fcm)/10)$^{0.3}$ GPA, $S_{r,max} = k3c + k1k2k4\emptyset/p_{p.eff}$

3.3. Deflection

The midspan deflections (δ_{max}) of the slabs were estimated according to CSA S806 2012 using Equation.7.

$\delta_{max} = \frac{PL^3}{48\,E_c I_{cr}}[3\left(\frac{a}{L}\right) - 4\left(\frac{a}{L}\right)^2 - 8(1 - \frac{I_{cr}}{I_g})(\frac{L_g}{L})^3]$ *(7)*

$Icr = bd^3k^3/3 + \eta_f A_f d^2(1-k)2$

$k = \sqrt{2\rho_f\rho\eta_f + (\rho_f\rho\eta_f)^2} - \rho_f\rho\eta_f$

4. RESULTS ANALYSIS AND DISCUSSION

4.1 Modes of failure and crack distribution

Throughout the test, loading was paused at intervals to visually inspect and record the progression of cracking, allowing for precise correlation between crack development and load levels. The failure modes were classified based on these visual assessments. A summary of crack initiation and propagation is provided in Table 6 and Figure 15. Notably, the initial crack width was approximately 0.005 mm at 44.1 kN, increasing to around 0.10 mm at 112.5 kN, and reaching 0.29 mm at the ultimate failure load of 130.8 kN, as shown in Figure 16. These initial cracks appeared simultaneously at the bottom surface beneath both loading points, as illustrated in Figures 16 and 17. As the applied load increased, diagonal cracks inclined at approximately 45° began to form near the right loading region. The number, width, and depth of cracks progressively increased with continued loading. At 91.2 kN, cracks had propagated to the top surface of the slab, with their orientation becoming increasingly inclined toward the right loading point. Eventually, at 130.8 kN, the slab failed due to shear.

Table 6: Crack formation and propagation behavior of simply supported one way slab under Four-point bending test

Slab ID	Initial crack			Maximum crack			No. of crack	Failure mode
	Load (KN)	Cracking moment (KN.m)	Crack width (mm)	Load (KN)	Ultimate moment (KN.m)	Crack width (mm)		
S30	44.1	8.8	0.005	130.8	26.2	0.29	14	S.F
S70	56.9	11.4	0.009	156.1	31.2	0.31	14	S.F
F30	39.2	7.8	0.06	103.1	20.6	1.26	20	S.F
F70	39.2	7.8	0.12	123.0	24.6	1.44	13	S.F with R-Bond-F

S.F: Shear Failure
R-Bond-F: GFRP rupture and bond failure.

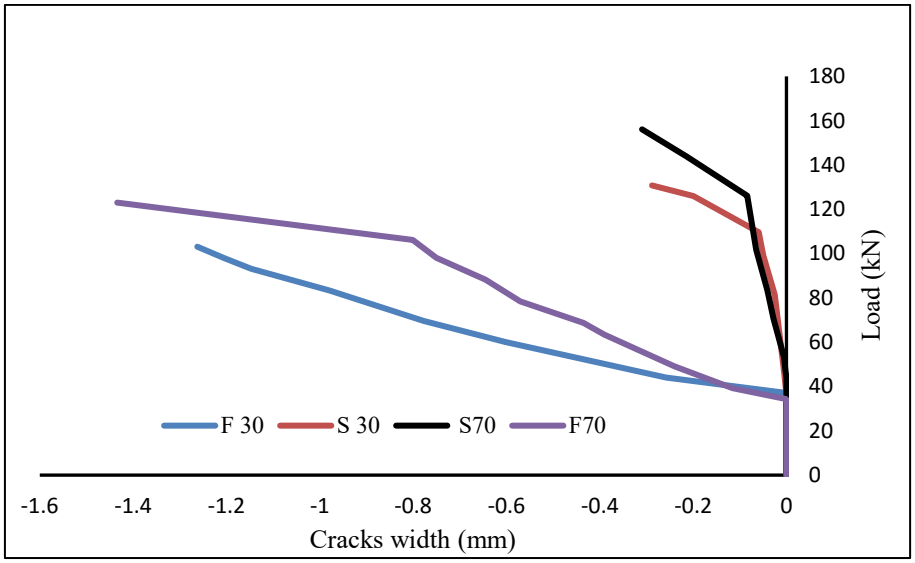

Figure 15: Crack width behavior of simply supported one way slab under Four-point bending

Figure 16: Crack patterns on the surface side of the slab (S30)

Figure 17: Crack patterns on the bottom surface of the slab (S30)

Figures 18 and Figures 19 illustrate the failure mode of slab S70 under a four-point bending test. Similar to slab S30, the first flexural crack in S70 appeared at the bottom surface near the center of the slab when the applied load reached approximately 56.9 kN. With further loading, vertical and diagonal cracks—inclined at about 45°—developed around the central and loading regions. As the load increased, these cracks grew in width, and their number remained comparable to those observed in slab S30. The slab ultimately failed due to

shear at the left support at a peak load of 156.1 kN. The initial crack width in slab S70 was recorded at 0.009 mm near the load point (Figure 17). This width gradually increased with loading, reaching 0.31 mm at failure. Compared to slab S30, slab S70 exhibited a slightly larger maximum crack width and significantly higher load-carrying capacity, approximately 1.07 and 1.20 times greater than that of S30.

Figure 18: Crack patterns on the surface side of the slab (S70)

Figure 19: Crack patterns on the other surface side of the slab (S70)

n slab F30, reinforced with GFRP bars, the first vertical cracks appeared at the center and right side of the loading point at 39.2 kN, as shown in Figure 20. With increasing load, vertical flexural cracks expanded in both size and number. At 83.3 kN, cracks extended to the slab's top surface and gradually inclined toward the load application zone. Shear failure occurred simultaneously at the left and right supports at 103.1 kN, as illustrated in Figure 20. Compared to slabs S30 and S70, slab F30 exhibited a distinctly different cracking pattern. The initial crack load was approximately 0.88 times lower than that of S30, while the initial crack width was 12 times greater. As loading progressed, crack width increased rapidly, and diagonal cracks formed near both supports, indicating a more brittle failure mode (Table 6, Figures 20 and 21). Crack width reached 1.0 mm at 83.4 kN, then crack width increased rapidly and reached 1.26 mm at 103.1 kN (failure load), Cracks increased in width and number which is more than cracks occurred in slab (S30) by 4.34 and 1.43 time, respectively.

Figure 20: Crack patterns on the surface side of the slab (F30)

Figure 21: Crack patterns on the other surface side of the slab (F30)

Figure 22 presents the failure mode of slab F70, which, similar to slab F30, experienced initial cracking at an applied load of 39.2 kN. The first crack appeared beneath the left support. As the load increased, five vertical flexural cracks formed, which progressively inclined toward the left loading point. At a load of 123.0 kN, the slab failed in diagonal tension. The final failure was preceded by an audible rupture, indicating

GFRP bar failure at the slab's bottom. As shown in Figure 23, the failure was attributed to a combination of GFRP rupture and bond failure between the reinforcement and concrete. However, F70 exhibited twice the initial crack width (0.12 mm) compared to F30 and a significantly larger maximum crack width of 1.44 mm at failure. It also had the lowest number of cracks among all tested slabs, suggesting a more brittle behavior.

Finally, GFRP-reinforced slabs (F30 and F70) demonstrated crack widths approximately 4.34 and 4.64 times greater than those of their steel-reinforced counterparts (S30 and S70), respectively. This behavior is attributed to the lower modulus of elasticity and brittle rupture characteristics of FRP materials.

Additionally, slabs made with high-strength concrete (S70 and F70) showed slightly greater crack widths—1.14 and 1.07 times larger, respectively—than normal-strength slabs (S30 and F30), likely due to the dense matrix and reduced micro cracking of high-strength concrete under stress, which often results in a more brittle bond failure mechanism.

Figure 22: Crack patterns on the surface and bottom side of the slab (F70)

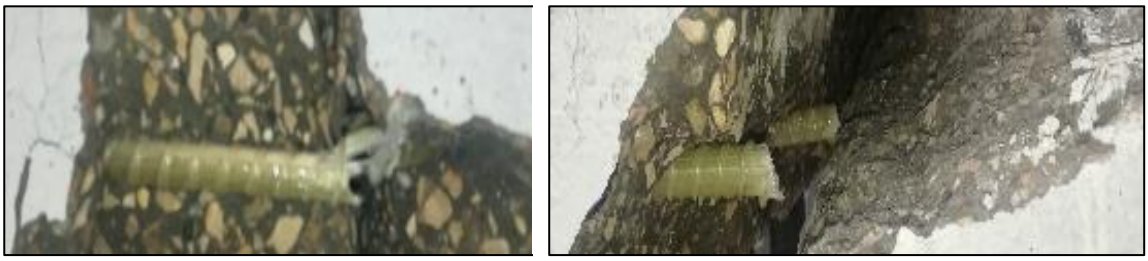

Figure 23: FRP rupture

This finding is supported by [35-38,20] whose concluded that FRP-reinforced elements typically exhibit greater crack widths compared to steel-reinforced members.

4.2 Load- Deflection Behavior

An experimental investigation was conducted on four reinforced concrete slabs using a 50-ton capacity load cell to evaluate the effect of applied load on their behavior and ultimate load-bearing capacity. The load-deflection behavior was assessed through a Four-Point Bending test. Deflection measurements were taken using three Linear Variable Differential Transformers (LVDTs) placed at the mid-span and two edge points of each slab. The LVDTs recorded nearly identical displacement values, indicating consistent deformation across the measurement points. Table 7 summarizes the recorded load and deflection data. Figure 24 presents the mid-span deflection behavior, while Figure 25 shows the edge-span deflection versus load response for the tested slabs.

Slab S30 exhibited a linear load-deflection response up to a load of 117.7 kN and a corresponding deflection of 4.8 mm, which is approximately 2.7 times greater than the load at first cracking. Beyond this point, the load-deflection curve became nonlinear, indicating the development of cracks within the concrete and the onset of steel reinforcement yielding. As the internal steel began to yield, the slab experienced large deflections with minimal load increase, reaching an ultimate load capacity of 130.8 kN at a deflection of 10.14 mm. Following sufficient plastic deformation, a sharp drop in the load-deflection curve was observed, signifying structural failure

The deflection behavior of slab S70 was similar to that of slab S30, but with an increase in both ultimate load and deflection by approximately 1.20 and 1.60 times, respectively. Slab F30, reinforced with GFRP bars, exhibited an almost linear load-deflection response up to failure. Initial deflection was recorded at approximately 19.2 kN, corresponding to 50% of the first crack load, which may be attributed to the lower modulus of elasticity of GFRP bars compared to steel reinforcement. The deflection behavior of slab F70, which was also reinforced with GFRP bars but used high-strength concrete, followed a similar linear trend to F30. However, in F70, deflection initiated at the first crack load and increased more rapidly with applied load,

ultimately showing the highest deflection among all tested slabs.

Table 7: Deflection values at Mid and Edge span

Slab ID	Ultimate Load (kN)	$\Delta_{exp.}$ (mm) mm	
		(Mid span)	(Edge span)
S30	130.8	10.14	13.13
S70	156.1	15.91	15.12
F30	103.1	26.2	26.2
F70	123.0	41.3	38.5

Slabs F30 and F70, reinforced with GFRP bars, recorded lower ultimate loads of 103.1 kN and 123.0 kN, respectively, compared to their corresponding control slabs. This represents a reduction of approximately 21.0% and 32.0% in ultimate load relative to slabs S30 and S70, which were reinforced with steel. Conversely, the mid-span deflection of the GFRP-reinforced slabs was significantly higher—approximately 2.6 times greater—than that of the corresponding steel-reinforced slabs. These findings are consistent with previous studies. For instance, [39] reported a 39% reduction in ultimate load capacity, which was attributed to a low reinforcement ratio that led to the rupture of GFRP bars. Similarly, [25]observed a 42% decrease in the ultimate load capacity of slabs reinforced with GFRP bars, compared to those reinforced with steel bars of equivalent area and distribution. This reduction was primarily attributed to premature concrete failure caused by excessive end slip of the GFRP reinforcement.

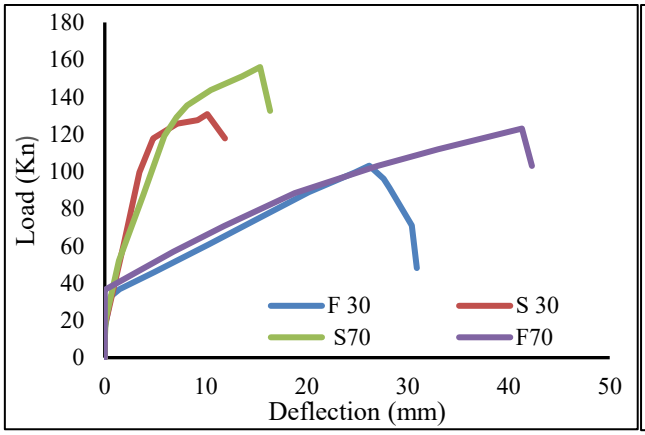

Figure 24: Load - deflection curves at mid- span

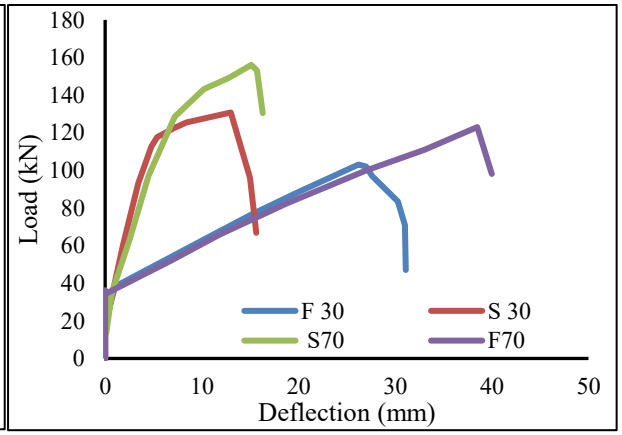

Figure 25: Load - deflection curves at edge- span

4.3 Strain Behavior

4.3.1 Concrete strains

Strains in the concrete were measured from gauges affixed to the top surface of the slab, as shown in Figure 9. The load–strain behavior is detailed in Table 8 and graphically represented in Figure 26. For slab S30, no strain was observed prior to cracking. At a load of 25.1 kN, the strain sharply increased to 1283 micro-strains without further load, indicating that crack propagation occurred at a lower load than crack initiation. As loading progressed, strain increased linearly up to 1956 micro-strains. Beyond this point, the curve exhibited zigzag behavior, corresponding to progressive cracking. The slab reached an ultimate load of 130.8 kN with a maximum strain of 3667.9 micro-strains. This type of strain is supported by [40].

Table 8: Concrete strain for tested specimens

Slab ID	Ultimate Load (kN)	Maximum Strain (micro-strains)
S30	130.8	3667.9
S70	156.1	1809
F30	103.1	1808
F70	123.0	1809

The strain behavior of high-strength concrete slab S70 began at a load of 54.0 kN, slightly before its cracking load, with a steep slope similar to slab S30, until strain of 258 micro-strains. The curve then transitioned into a zigzag pattern, indicating progressive cracking, and continued up to the ultimate load of 156.1 kN with a maximum strain of 1809.0 micro-strains. Slab F30 initiated strain near its cracking load at 34.0 kN and

exhibited a nearly linear trend up to 84% of its failure load. It ultimately failed at 103.1 kN with a strain of 1808 micro-strains, which is lower than strain of slab (S30) by about 0.5 times. The strain curve of high strength concrete (F70) demonstrated also a steep slope at load from 52.0 kN and record 516 micro-strains at load 32.2 KN. After that the strain curve began to increase as zigzag line like slab (S70) up to the ultimate load capacity of 123.0 kN and strain of 1809.0 micro-strains.

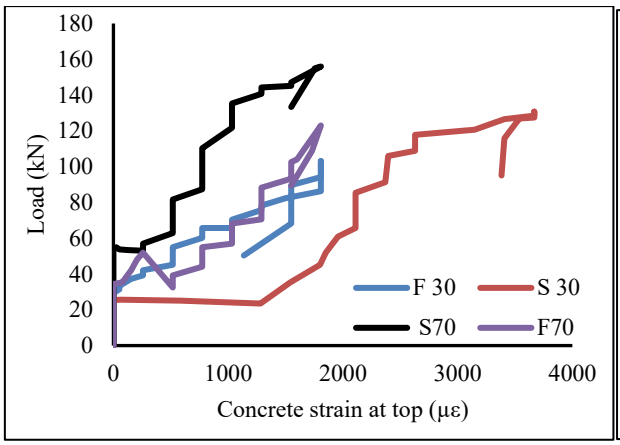

Figure 26: Concrete strain in the top of the slabs near mid-span

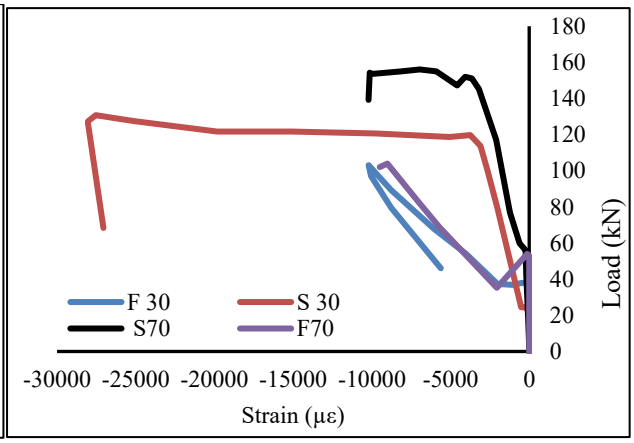

Figure 27: Load-strain for longitudinal steel and GFRP bars

4.3.2 Steel and GFRP bar strains

Strain gauges were attached to the longitudinal steel and GFRP rebars at the slab edges and mid-span to monitor strain during the full loading sequence as shown in Figure 7. The load–strain behavior of the reinforcements is presented in Table 9 and Figure 27. In slab S30, the bottom steel reinforcement exhibited nearly zero strain before concrete cracking. At a load of 24.5 kN (prior to cracking), the strain curve began with a steep slope and increased linearly up to 3085 micro-strains at 113.8 kN. As loading continued, the curve slightly deviated, and strain in the steel rose rapidly. Yielding occurred at 3750 micro-strains, followed by a significant increase in strain with minimal load increments, reaching a maximum of 28,034 micro-strains.

Table 9: Steel and GFRP bars strain.

Slab ID	Ultimate load (kN)	Strain at Yield Strength (micro-strains)	Maximum strain (micro-strains
S30	130.8	3750	28034
S70	156.1	3653.7	10135
F30	103.1	-	10053
F70	123.0	-	9009

The load–strain curve of high-strength slab S70 showed a different behavior compared to slab S30, as it sustained more load before the steel began to yield. Strain in the steel reinforcement started at the initial cracking load of 54.0 kN and increased linearly up to approximately 97% of the ultimate load. This behavior is likely due to the high-strength concrete carrying most of the load after cracking. During this stage, steel strain remained nearly zero, and the curve stayed close to the vertical axis. A significant rise in strain was observed afterward, even with minimal additional loading. As the load increased further, the strain response became nonlinear, reaching a peak value of 10,135 micro-strains at failure**.** The strain curve of slab F30, reinforced with GFRP bars, began at a load of 39.5 kN, approximately corresponding to the first cracking load. The curve initially showed a slight nonlinear drop, reaching 2058 micro-strains at a reduced load of 35.3 kN. With further loading, the strain increased linearly up to the failure load of 103.1 kN, reaching a maximum strain of 10053 micro-strains, which is approximately 2.75 times higher than that of the corresponding steel-reinforced slab. In slab F70, the bottom GFRP bars showed nearly zero strain up to 53.0 kN—similar to slab S70. Beyond this point, the load strain curve behaved similarly like strain of slab (F30), the GFRP bars in slab F70 recorded a peak strain of 9009 micro-strains at the point of failure.

5. Comparison of Experimental Results with theoretical

5.1 Flexural Capacity

In this study, the Crack moment (*Mcr*) and the Nominal moment capacity (*Mn*) were calculated using formulations in the CSA S806-12 code.

We note that there was no structural design code (including CSA S806-12, ACI 318 or Eurocode 2) directly includes the effect of loading type (point load, 2-

point load and UDL) in the cracking moment formula**.** Nominal load capacities from CSA S806-12 were calculated using the equation ($P_n = 2M_n/a$) , applicable to three-point loading. This is similar calculation by [31]. Table 10 provides the experimental and predicted experimental cracking moment and Ultimate moment with CSA S806-12 of simply supported one-way slab under three-point loading.

The first-crack moment values were determined and found to lie within the range of 7.8 to 11.4 kN·m. The predicted and experimental moment capacities at both cracking and ultimate load levels showed good agreement for all slabs. However, the F70 slab reinforced with GFRP exhibited slightly unconservative behavior at the cracking moment stage. According to CSA S806-12, the average ratio of experimental to predicted moment capacity was 0.81 ± 0.09 and 0.85 ± 0.18 for cracking moments.

Table 10: Comparison of predicted and experimental cracking and nominal moments capacity

Slab ID	Load (kN)	Crack moment (*Mcr*)			Load P_n (kN)	Nominal moment capacity (*Mn*)		
		Exp. (kN.m)	Pred. (kN.m)	Exp/Pred		Exp. (kN.m)	Pred. (kN.m)	Exp/Pred
S30	44.1	8.8	8.6	1.02	130.8	26.2	35.1	0.75
S70	56.9	11.4	13.1	0.87	156.1	31.2	38.2	0.82
F30	39.2	7.8	8.6	0.91	103.1	20.6	28.0	0.74
F70	39.2	7.8	13.1	0.60	123.0	24.6	26.4	0.93
Mean				0.85				0.81
Stand. Dev.				0.18				0.09

5.2. Crack width

Crack width calculations in this study were based on the provisions outlined in CSA S6-06 [41], ACI 440.1R-06 [27] and EURO EN 1992-1-1:2004 code [42]. Experimental crack widths were compared with theoretical predictions (Table 11).

Table 11: Comparison of predicted and experimental crack width of simply supported one-way slab under three-point loading

Slab ID	Load (kN)	Crack width- (mm)						
		Experimental mximum crack	ACI 440.1R-06		CSA S6-06		EURO EN 1992-1-1:2004	
		(w_{exp})	(w_{pred})	(w_{exp} / w_{pred})	(w_{pred})	(w_{exp} / w_{pred})	(w_{pred})	(w_{exp} / w_{pred})
S30	130.8	0.29	0.22	1.31	0.14	2.06	0.30	0.95
S70	156.1	0.31	0.22	1.41	0.14	2.23	0.37	0.84
F30	103.1	1.26	1.02	1.24	0.64	1.96	1.50	0.84
F70	123.0	1.44	1.02	1.42	0.64	2.23	1.84	0.78
Mean				1.34 0.08		2.12 0.13		0.85 0.07
Stand. Dev.				0.08		0.13		0.07

ACI and CSA do not directly consider concrete strength (fcu) in crack width formulas but account for it indirectly through bond and stiffness factors. Therefore, there is a negligible difference in crack width when increasing the strength of concrete from 30 to 70 MPA. ACI equations were accurate for normal strength slabs (S30, F30) but slightly unconservative for high-strength slabs (S70, F70), with an average experimental-to-predicted ratio of 1.34 ± 0.08. CSA equations performed poorly for all slabs, with a ratio of 2.12 ± 0.13. In contrast, EURO EN 1992-1-1:2004 explicitly includes concrete strength and showed the best correlation, with a ratio of 0.85 ± 0.07.

5.3. Deflection

The midspan deflections (δ_{max}) of the slabs were calculated using formulations in the CSA S806 2012 and results reported in Table 12. Mid-span deflection predictions closely matched experimental results across all tested slabs, demonstrating good agreement with CSA S806-12 provisions. An average experimental-to-predicted deflection ratio of 0.92 ± 0.09 was recorded, indicating that the code provides a reliable estimation of slab deflection under loading conditions.

Table 12: Comparison between experimental and prediction Mid span deflection, as per CSA S806 2012

Slab ID	Ultimate Load (kN)	Mid span	CSA2012	
		Δ exp. (mm)	Δpred.(mm)	Δ exp./pred.
S30	130.8	10.14	11.77	0.86
S70	156.1	15.91	15.27	1.04

F30	103.1	26.2	30.57	0.86
F70	123.0	41.3	43.97	0.94
Mean				0.92
Stand. Dev.				0.09

6. CONCLUSIONS

This paper experimentally investigated the flexural behavior of (HSC) and (NSC) simply supported one-way slab reinforced with (GFRP) bars under Four Point Bending test. The ultimate load capacity, crack patterns, failure modes, ultimate deflection, concrete and GFRP/ steel bar strains, was obtained**.** Considering the experimental and analytical results, the following conclusions are presented

1. Steel-reinforced slabs exhibited ductile flexural failure initiated by steel yielding, followed by shear failure. In contrast, GFRP-reinforced slabs failed through GFRP rupture, then shear failure.
2. GFRP-reinforced slabs (F30 and F70) exhibited significantly wider cracks than steel-reinforced slabs (S30 and S70) by 4.34 and 4.64, respectively. Crack widths in high-strength slabs (S70 and F70) were slightly greater than those in normal-strength slabs by 1.14 and 1.07 times. Additionally, slabs F30 and F70 showed reduced ultimate loads—21.0% and 32.0% lower than the control slabs—while mid-span deflections were approximately 2.60 times greater than their steel-reinforced counterparts.
3. At the failure load level, steel-reinforced slabs (NSC and HSC) exhibited higher strain values than GFRP-reinforced slabs by 2.75 and 1.12 respectively.
4. The predicted and experimental moment capacities at both cracking and ultimate load levels showed good agreement for all slabs. However, the F70 slab reinforced with GFRP exhibited slightly unconservative behavior at the cracking moment stage. According to CSA S806-12, the average ratio of experimental to predicted moment capacity was 0.81 ± 0.09 and 0.85 ± 0.18 for cracking moments.
5. The ACI crack width equations provided acceptable predictions for normal-strength concrete slabs (S30 and F30) but were slightly unconservative for high-strength slabs (S70 and F70). In contrast, the CSA code equations were not suitable for all slabs, with an average experimental-to-predicted crack width ratio of 2.12 ± 0.13. The EURO EN 1992-1-1:2004 code, which explicitly considers concrete strength through parameters through *fct*, *Ec* and bond factor, showed better alignment with both normal and high-strength slab results. It achieved an average experimental-to-predicted crack width ratio of 0.85 ± 0.07, indicating good agreement.
6. Mid-span deflection predictions closely matched experimental results across all tested slabs, demonstrating good agreement with CSA S806-12 provisions. An average experimental-to-predicted deflection ratio of 0.92 ± 0.09 was recorded, indicating that the code provides a reliable estimation of slab deflection under loading conditions.

Notations:

fr = modulus of rupture in Mpa
fc = compressive strength of concrete in MPa
λ = modification factor based on concrete density. In the case of normal-weight concrete, λ =1.
p_f = reinforcement ratio
p_{fb} = FRP reinforcement ratio producing balanced
Mn = Nominal flexural capacity
a = length between a 50mm Round structural steel solid bars and near support
w_{cr} = crack width at the tensile surface of the flexural element (mm)
f_f = reinforcement stress, psi or MPa
E_f = Elastic modulus of the reinforcing material (psi or MPa)
h_2 = distance from the extreme tension face of the section to the neutral axis
h_1 = depth from the tension steel or FRP bars to the neutral axis
dc = Distance from the extreme tension face to the centroid of the closest reinforcement bar
s = spacing of reinforcement bars
k_b = bond factor that reflects the effectiveness of the bond between the FRP reinforcement and the adjacent concrete. For FRP bars exhibiting bond behavior comparable to that of uncoated steel bars.
w = maximum width of a crack, in. or mm
β = Ratio of the distance from the neutral axis to the tension face, to the distance from the neutral axis to the centroid of the reinforcement.
$S_{r,max}$ = maximum crack spacing
ε_{sm} = Mean tensile strain in the reinforcement due to the relevant combination of applied loads
ε_{cm} = Mean concrete strain between cracks
σs = Stress developed in the tensile reinforcement in a cracked section analysis
α_e = Represents ratio
Ø = Bar diameter.
A_f = Total area of the FRP reinforcement
k_1 = A coefficient that accounts for the bond characteristics of the bonded reinforcement. It is taken as 0.8 for high-bond (deformed) bars and 0.6 for bars with an effectively plain surface, k_2: A coefficient that accounts for the distribution of strain, it is taken as 0.5 for members in bending and 1.0 for members subjected to pure tension.

k3, k4 = Recommended design coefficients 3.4 and 0.425
kt = load duration factor is 0.6 for short-term and 0.4 for long-term loading.
Icr = Moment of inertia of the equivalent cracked section
d = effective depth
η_f = Ratio of the elastic modulus of the FRP reinforcement (E_f) to the elastic modulus of the concrete (E_c)
$\varepsilon_{cu:}$ = concrete strain
k = ratio of the depth of the neutral axis to the effective depth of reinforcement.
L = span length
Lg = length from the support to the point where *Ma* = *Mcr*
Ma= *maximum* moment in member at stage deflection
Mcr= cracking moment

Conflict of interest: The authors declare that they have no conflicts of interest.

Data availability:

The data supporting the findings of this study are available from the corresponding authors upon reasonable request.

Funding: Not Applicable.

Ethics, Consent to Participate, and Consent: Not Applicable.

REFERENCES

1. Harle, S., Glass Fiber Reinforced Concrete & Its Properties. INTERNATIONAL JOURNAL OF ENGINEERING SCIENCES & RESEARCH TECHNOLOGY 2014.
2. Stuart, V., L.S.J.P.o.t.I.o.C.E.-S. Cunningham, and Buildings, FRP reinforced-concrete slabs: a comparative design study. Proceedings of the Institution of Civil Engineers-Structures and Buildings, 2017. 170(8): p. 581-602.
3. Gautam Jain1, T.S., Naveen Kumar3, Navneet Kumar4,Ruby Pant4, A STUDY OF FIBERGLASS MATERIAL WITH DIFFERENT COMPOSITIONS, in International Conference on Advances in Engineering Science Management & Technology (ICAESMT)-2019, Uttaranchal University, Dehradun, India 2019.
4. Granju, J.-L., S.U.J.C. Balouch, and C. Research, Corrosion of steel fibre reinforced concrete from the cracks. Cement and Concrete Research 2005. 35(3): p. 572-577.
5. Yu Zheng , G.Y., Yunfeng Pan, Investigation of ultimate strengths of concrete bridge deck slabs reinforced with GFRP bars. Construction and Building Materials, 2012. 28(1): p. 482-492.
6. Selvaraju, Y.R., REVIEW ON BEHAVIOUR OF GLASS FIBRE REINFORCED POLYMER RC MEMBERS, in International Conference on Explorations and Innovations in Engineering & Technology. 2016.
7. Fuhaid, A.F.A. and A.J.B. Niaz, Carbonation and corrosion problems in reinforced concrete structures. Buildings, 2022. 12(5): p. 586.
8. Ifrahim, M.S., A.J. Sangi, and S.H. Ahmad. Experimental and numerical investigation of flexural behaviour of concrete beams reinforced with GFRP bars. in Structures. 2023. Elsevier.
9. Patil, V.R.J.I.J.I.R.A.E., Experimental Study of Behavior of RCC Beam by Replacing Steel Bars with Glass Fiber Reinforced Polymer and Carbon Reinforced Fiber Polymer (GFRP). Int. J. Innov. Res. Adv. Eng, 2014. 1: p. 205-210.
10. Ombres, L., T. Alkhrdaji, and A. Nanni. Flexural analysis of one way concrete slabs reinforced with GFRP rebars. in International meeting on composite materials, PLAST. 2000. Citeseer.
11. Masmoudi, A., et al., New parameter design of GFRP RC beams. Construction and Building Materials 2012. 29: p. 627-632.
12. Yoo, D.-Y., N. Banthia, and Y.-S.J.C.P.B.E. Yoon, Predicting service deflection of ultra-high-performance fiber-reinforced concrete beams reinforced with GFRP bars. Composites Part B: Engineering, 2016. 99: p. 381-397.
13. Li-xiang, S., et al. Experimental study on flexural behavior of GFRP reinforced concrete slabs. in IOP Conference Series: Earth and Environmental Science. 2021. IOP Publishing.
14. Kalpana, V., K.J.J.o.r.p. Subramanian, and composites, Behavior of concrete beams reinforced with GFRP BARS. Journal of reinforced plastics and composites 2011. 30(23): p. 1915-1922.
15. Sivagamasundari, R. and G.J.T.O.C.E.J. Kumaran, A comparative study on the flexural behaviour of one-way concrete slabs reinforced with GFRP reinforcements and conventional reinforcements when subjected to monoTonic and repeated loading. The Open Civil Engineering, 2008. 2(1): p. 24-34.
16. El-Ragaby, A., E. El-Salakawy, and B.J.J.o.C.f.C. Benmokrane, Fatigue life evaluation of concrete bridge deck slabs reinforced with glass FRP composite bars. Journal of Composites for Construction 2007. 11(3): p. 258-268.
17. SARIKAYA, H. and H.E. BALCIOĞLU, THE EFFECT OF GLASS FIBER REBAR REINFORCEMENT ON FLEXURAL BEHAVIOUR OF REINFORCED CONCRETE STRUCTURAL ELEMENTS. 2018.
18. Abdalla, H.J.c.s., Evaluation of deflection in concrete members reinforced with fibre reinforced polymer (FRP) bars. composite structures 2002. 56(1): p. 63-71.
19. Chang, K., D.J.J.o.A.A. Seo, and B. Engineering, Behavior of one-way concrete slabs reinforced with GFRP bars. 2012. 11(2): p. 351-358.
20. Sdiri, A., et al., Comparative Study of GFRP and Steel Rebar Bonding in Concrete: Experimental Analysis and Crack Prediction. Journal of

Composite & Advanced Materials/Revue des Composites et des Matériaux Avancés, 2024. 34(2).
21. Adam, M.A., et al., Structural Behavior of High-Strength Concrete Slabs Reinforced with GFRP Bars. Polymers (Basel), 2021. 13(17): p. 2997.
22. Abdul-Salam, B., et al., Mechanisms of shear resistance of one-way concrete slabs reinforced with FRP bars. Construction and Building Materials, 2016. 127: p. 959-970.
23. El-Nemr, A., E.A. Ahmed, and B.J.A.s.j. Benmokrane, Flexural Behavior and Serviceability of Normal-and High-Strength Concrete Beams Reinforced with Glass Fiber-Reinforced Polymer Bars. ACI structural journal, 2013. 110(6).
24. Kabashi, N., et al. Flexural behavior and cracks in concrete beams reinforced with GFRP bars. in International Congress on Polymers in Concrete (ICPIC 2018) Polymers for Resilient and Sustainable Concrete Infrastructure 16. 2018. Springer.
25. Lotfy, E.M., S.M. Elzeiny, and A.M.J.P.o.t.I.o.C.E.-C.M. Rashad, Flexural capacity of one-way GFRP concrete slabs. Proceedings of the Institution of Civil Engineers-Construction Materials 2011. 164(3): p. 143-152.
26. Daoud, O. and A.J.F.J.o.E.S. Fadul, Shear behavior in beams reinforced with glass-fiber reinforced polymer bars (GFRPB) without stirrups. FES Journal of Engineering Sciences, 2020. 9(1): p. 72-78.
27. Alkhrdaji, T., et al., Guide for the design and construction of structural concrete reinforced with FRP bars. Proc., American Concrete Institute (ACI) Committee 2006. 440.
28. Wang, H. and A.J.A.S.J. Belarbi, SP230, Flexural behavior of fiber-reinforced-concrete beams reinforced with FRP rebars. ACI Structural Journal, SP230 2005. 51(230): p. 895-914.
29. Al-Rubaye, M., et al., Flexural behaviour of concrete slabs reinforced with GFRP bars and hollow composite reinforcing systems. Composite structures 2020. 236: p. 111836.
30. Yoo, D.-Y., N. Banthia, and Y.-S.J.E.S. Yoon, Flexural behavior of ultra-high-performance fiber-reinforced concrete beams reinforced with GFRP and steel rebars. Engineering Structures, 2016. 111: p. 246-262.
31. GoldsTon, M., et al., Flexural behaviour of GFRP reinforced high strength and ultra high strength concrete beams. Construction and Building Materials, 2017. 131: p. 606-617.
32. Jabbar, S.A. and S.B.J.K.i.j.o.m.s. Farid, Replacement of steel rebars by GFRP rebars in the concrete structures. Karbala international journal of modern science, 2018. 4(2): p. 216-227.
33. Al-Jabri, K.S., et al., Copper slag as sand replacement for high performance concrete. Cement and concrete composites 2009. 31(7): p. 483-488.
34. CSA, Canadian Standards Association, Design and Construction of Building Structures with Fibre-Reinforced Polymers, American Concrete Institute, Ontario, Canada, 2012, pp. S806–S812. 2012.
35. Michaluk, C.R., et al., Flexural behavior of one-way concrete slabs reinforced by fiber reinforced plastic reinforcements. ACI structural Journal 1998. 95: p. 353-365.
36. Hassan, T., et al., Fibre reinforced polymer reinforcing bars for bridge decks. Canadian journal of civil engineering, 2000. 27(5): p. 839-849.
37. Zhang, B., et al., Behaviour of one-way concrete slabs reinforced with CFRP grid reinforcements. Construction and Building Materials 2004. 18(8): p. 625-635.
38. Tharmarajah, G., S. Taylor, and D. Robinson, Experimental and Numerical Investigation of Compressive Membrane Action in GFRP-Reinforced Concrete Slabs. Polymers (Basel), 2023. 15(5): p. 1230.
39. Adam, M., et al., Structural Behavior of High-Strength Concrete Slabs Reinforced with GFRP Bars. Polymers 2021, 13, 2997. Polymers (Basel), 2021. 13(17): p. 2997.
40. Carreira, D.J. and K.-H. Chu. Stress-strain relationship for reinforced concrete in tension. in Journal Proceedings. 1986.
41. CSA, , "Canadian Highway Bridge Design Code," Canadian Standard Association, Rexdale, ON, Canada. 2006.
42. Eurocode2, E. EN1992 Eurocode 2: Design of concrete structures. in Proceedings of the Institution of Civil Engineers-Civil Engineering. 1992. Thomas Telford Ltd.